UNCORRECTED and UNAPPROVED version (submitted manuscript)

For the final, citable paper please see https://doi.org/10.1021/acsami.6b11436

TiO_2 Nanotubes Arrays Loaded with Ligand-free Au Nanoparticles: Enhancement in Photocatalytic Activity

Marcello Marelli[†], Claudio Evangelisti[†*], Maria Vittoria Diamanti[‡], Vladimiro Dal Santo[†], Maria Pia Pedeferri[‡], Claudia L. Bianchi[/], Luca Schiavi[§] and Alberto Strini[§]

[†] Istituto di Scienze e Tecnologie Molecolari (ISTM-CNR), via Golgi, 19, 20133 Milano, Italy

‡ Department of Chemistry, Materials and Chemical Engineering 'Giulio Natta', Politecnico di Milano,Via Mancinelli 7, 20131 Milan, Italy

/ Dipartimento di Chimica, Università di Milano, Via Golgi 19 — 20133 Milano, Italy

[§] Istituto per le Tecnologie della Costruzione (ITC-CNR), via Lombardia, 49, I-20098 San Giuliano Milanese (MI), Italy

Corresponding author: Dr. Claudio Evangelisti; Istituto di Scienze e Tecnologie Molecolari (ISTM-CNR), Via C. Golgi 19, 20133 Milano (ITALY)- phone: +390250995623

email: claudio.evangelisti@istm.cnr.it

Abstract

A new protocol to synthesize size-controlled Au nanoparticles (NPs) loaded onto vertically aligned anatase TiO_2 nanotubes arrays (TNTAs) prepared by electrochemical anodization is reported. Ligand-free Au NPs (< 10 nm) were deposited onto anatase TNTAs supports, finely tuning the Au loading by controlling the immersion time of the support into metal vapor synthesis (MVS)-derived Au-acetone solutions. The Au-TNTAs composites were characterized by electron microscopies (SEM, (S)TEM), X-ray diffraction, X-ray photoelectron spectroscopy and UV-Vis spectroscopy. Their photocatalytic efficiency was evaluated in toluene degradation in air at ambient conditions without thermal or chemical post-synthetic treatments. The role of Au loadings was pointed out, obtaining a three times enhancement of the pristine anatase TNTAs activity with the best sample containing 3.3 μg Au cm^{-2}.

UNCORRECTED and UNAPPROVED version (submitted manuscript)

For the final, citable paper please see https://doi.org/10.1021/acsami.6b11436

1. Introduction

Titanium dioxide (TiO_2) is the most diffused among photocatalytic material thanks to its photo-reactivity (band-gap of 3.2eV and 3.0 eV for the anatase and rutile phase, respectively), high stability, non-toxicity, and availability [1-2]. Under UV light nanostructured TiO_2 is able to promote a wide range of reactions such as hydrogen production by water splitting [3], electricity production in dye sensitized solar cells [4], CO_2 reduction [5]. Moreover, its capability to degrade organic pollutants such as VOCs [6] (benzene, toluene, organic chlorides) and inorganic pollutants [7] (NOx, SOx, NH_3, and CO) finds interesting applications for indoor and outdoor air purification [8-10]. However, the extremely low photocatalytic efficiency of conventional nanostructured TiO_2 powder (quantum yields < 1%) [11] involves the requirement of a large amount of material, the catalyst recycling is difficult in and, moreover, aggregation into larger and less active particles can occur. Recently, in order to overcome these drawbacks, intense efforts have been focused on the modification of the electronic properties of nanostructured TiO_2-based materials by different approaches, such as metal nanoparticles deposition, doping with metal and non-metal ions or coupling with other semiconductors [12-]. Among them, the loading of TiO_2-based materials with Au nanoparticles (NPs) has been extensively investigated by several research groups [13-15]. The hetero-junction between TiO_2 surface and Au NPs leads to a rapid interfacial photo-generated electron transfer from TiO_2 to Au NPs (Schottky barrier) increasing the separation of photogenerated e^-/h^+ pairs, reducing recombination probability and increasing therefore the photocatalytic activity [16-17]. The amplitude of this effect is strongly related to the particle size, since mainly the small ones (< 10 nm) result in higher efficiency, as well as to the Au loading [18-19]. Other mechanisms as gold surface plasmon resonance are often invoked to explain the enhanced photoactivity of these materials under visible light irradiation [20-23]. For the synthesis of Au NPs decorated TiO_2 different approaches have been reported, including conventional impregnation [24], deposition-precipitation [24-25], chemical reduction [26] and photodeposition [21,27].

Besides, in the last years, one-dimensional nanostructured TiO_2 such as nanotubes arrays (TNTAs) have attracted an increasing attention in (photo)catalysis due to their unique physico-chemical and structural properties [28-29]. TNTAs show a stable large surface-to-volume ratio (> 300 $m^2\ g^{-1}$) with no risk of aggregation, high sedimentation rate as well as excellent adhesion and electrical contact withthe metallic substrate from which they are originated [30-31]. Moreover, they are expected to have better photogenerated charge separation when compared to TiO_2 NPs due to the

UNCORRECTED and UNAPPROVED version (submitted manuscript)

For the final, citable paper please see https://doi.org/10.1021/acsami.6b11436

improved electron transportation along the1D channels and the decrement of inter-crystalline contacts [32].

The possibility to obtain TNTAs from the anodic oxidation of metallic titanium foils paves also the way to the direct realization of supported photocatalysts [33-35] without the drawbacks related to the sintering process of photoactive titania powders [36].

In order to combine the advantages of TNTAs systems with an active Au NPs decoration, conventional deposition methods are generally not effective due to fast formation of large metal aggregates, crystalline phase-changes or the required application of complex procedures which need careful cleaning steps and/or post-thermal treatments. Recently, advanced methodologies enabling the deposition of size-controlled Au NPs homogeneously dispersed onto geometrically ordered TNTAs have been reported [32-33]. Paramsivam *et al.* decorated TNTA with Au NPs by sputtering technique followed by post-annealing at high temperature (450°C) to ensure the Au NPs adhesion. The synthesis afforded Au NPs with diameters centered at 28 nm but post-thermal treatment led to the formation less active rutile phase [37]. Wu *et al.* adopted a pulse electrodeposition technique to deposit Au NPs with size ranging from 8 to 40 nm onto TNTAs electrodes [33]. Au NPs size was controlled by adjusting electrochemical parameters; however, a broadening of size distribution rather than an increase of particles number was observed by increasing the metal loading. Xiao *et al.* reported an innovative approach to the synthesis of Au NPs by solar light irradiation of metal cluster decorated TNTAs supports, obtaining binary hybrid nanocomposites with a mean Au particle size of 13 nm [35, 38].

Herein we propose a simple and scalable synthetic protocol able to load size-controlled (< 10 nm) Au NPs onto vertically aligned anatase TNTAs [34]. Au NPs were generated by the metal vapor synthesis technique (MVS) [39]. This method allows the preparation of Au NPs in acetone solution without the use of any additional stabilizing ligands. The Au NPs loading onto the TNTAs surface was easily controlled by changing the dipping time of the support without significant changes of Au NPs size distributions. The photocatalytic activity of these systems was assessed measuring the degradation of toluene in air at ppb level and in typical ambient condition. Toluene can be easily found both in indoor and outdoor polluted air and was hence selected as aromatic ambient pollutant model [40-41].

2. Experimental

TNTAs were produced by anodizing substrates of commercial purity titanium, grade 2 following ASTM classification [42]. Titanium sheets of approximately 10 cm x 10 cm area, 0.5 mm thickness

UNCORRECTED and UNAPPROVED version (submitted manuscript)

For the final, citable paper please see https://doi.org/10.1021/acsami.6b11436

were cleaned by degreasing with acetone, then immersed in a solution of 0.5 wt.% NaF/1M Na_2SO_4 and connected to an activated titanium counter electrode. Anodizing was performed by applying 20 V with a voltage ramp of 1 V s^{-1} and maintaining the chosen voltage for 6 h. After the treatment, samples were rinsed with deionized water to remove salt deposits from the electrolyte and thermally annealed in air at 400°C for 2 h: annealing was necessary to crystallize the obtained amorphous TiO_2 [34,43]. Finally, samples were cut to the desired size of 2.5 cm x 2.5 cm. BET measurements were performed by Kr physisorption at 77 K (ASAP 2020, Micrometitics). X-ray diffraction (XRD) measurements (Philips PW 3710-Cu Kα radiation) at room temperature were used to determine the crystal structure of the oxide.

Au NPs were synthesized by the MVS technique (Electronic Supplementary Information, ESI Fig. S1) following a previously reported procedure [44]. Au vapors generated at 10^{-4} mBar by resistive heating of a alumina crucible filled with ca. 500 mg of gold pellets, was co-condensed at liquid nitrogen temperature (-196°C) with acetone (100 ml) in the glass reactor chamber of the MVS apparatus in ca. 40 min. The reactor chamber was heated to the melting point of the solid matrix and the resulting deep purple solution was siphoned at low temperature in a Schlenk tube and kept in a refrigerator at -20 °C. The Au-content of the solvated metal atoms (SMA) solution was 5.0 mg mL^{-1}, as determined by ICP-OES (Thermo Scientific ICAP6300 Duo) analysis. For this work, 25 mL of Au SMA at 0.9 mg mL^{-1} were obtained by dilution from the pristine SMA solution with distilled acetone.

UV−vis diffuse reflectance spectra (DRS) were collected by an Avaspec 2048-L spectrometer (Avantes) equipped with a Deuterium-Halogen Light Source (AvaLight DHS) and a 30 mm diameter integrating sphere (Avasphere 30 REFL). A Diffuse PTFE material (Avantes WS-2) was used as reference tile. The X-ray photoelectron spectroscopy (XPS) characterizations were carried out by a M-probesystem (SSI - Surface Science Instruments); C1s was taken as internal reference for energy.

Scanning electron microscopy (SEM) characterization were performed at 15 kV in high vacuum mode with a PHILIPS XL30 ESEME-FEG. SEM-EDX elemental analysis (Energy Dispersive X-ray spectroscopy) were carried out by a EDAX Sirion 200/400 probe. EDS data were collected on a 5 μm^2 active area. Scanning transmission electron microscopy (STEM) and high resolution transmission electron microscopy (HRTEM) measurements were collected by using a LIBRA 200FE ZEISS at 200 kV equipped with a high angle annular dark field detector (HAADF). Sample were collected scratching the surface with a sharp scalpel and collecting the fragment onto a holey carbon supported Cu GRID by simple adherence [45]. Elemental quantitative analysis were performed by ICP-OES with external calibration, after complete Au dissolution in 2 mL of *aqua*

UNCORRECTED and UNAPPROVED version (submitted manuscript)

For the final, citable paper please see https://doi.org/10.1021/acsami.6b11436

regia solution at room temperature. The back side of each sample was covered by a protective polymeric acid-resistant layer: in this way only the gold on the front side (the active and tested side) was digested.

The Au NPs were loaded onto the TiO_2 surface by dipping the TNTAs coated samples directly in the Au-acetone SMA at room temperature under Ar inert atmosphere. The reactor was a conventional Schlenk glass tube with proper size to place upright the sample inside. In order to complete dip the sample slide, we used 25 mL of SMA solution (0.9 mg Au mL^{-1}). Different Au/TNTAs samples were prepared by varying the dipping time (2, 10, 120, 240, 480, 1200 minutes, respectively). After the deposition, the samples were washed by a rinsing cycle (deionized water-acetone-isopropanol-deionized water in sequence) and dried in air at room temperature. A schematic representation of the overall deposition procedure is reported Fig. S2. The photocatalytic activity was assessed measuring the toluene degradation with a previously described experimental system [40] based on a continuous-flow stirred photoreactor. The system was equipped with six fluorescent lamps (PL-S/BLB, Philips) as UV-A source resulting in 605 ± 20 μW cm^{-2} irradiance (340-400 nm range) and it was operated at constant toluene concentration (750 ± 50 nmol m^{-3}) allowing a direct comparison of the obtained reaction rates. All the measurements were carried out at 25 ± 0.2 °C and 50 ± 2 R.H. (errors as 1 σ repeatability). Further details are reported in Fig. S3. All samples were catalytically tested before and after the Au NPs loading.

3. Result and Discussion

In order to synthesize separately the TNTAs supports and the Au NPs we used two well-established and supported methodologies (i.e. electrochemical-anodization and MVS respectively).

TNTAs obtained by metallic titanium foil anodization offer the benefit of growing an oxide layer well anchored to the metallic substrate. Scanning electron microscopy (SEM) of the bare TNTAs showed their nanotubular features containing self-organized nanotubes on the surface clearly separated from one another with inner mean diameter of 50 nm (Fig. S2d). The film thickness, measured from cross section SEM image, (Fig. S2e) was estimated around 1 μm. BET measurements highlight a grow of 95 square meter of exposed surface area every square meter of geometrical slide area. After annealing, only TiO_2-anatase phase structure was detected by XRD analyses (Fig. S4). Each sample was checked for anatase purity before Au deposition in the angular range $20°<2\theta<30°$.

As previously reported [39 ,46-47], the controlled co-condensation of Au vapors and acetone vapors by means MVS technique affords mainly spherical Au nanoclusters with size less than 10 nm in

UNCORRECTED and UNAPPROVED version (submitted manuscript)

For the final, citable paper please see https://doi.org/10.1021/acsami.6b11436

diameter weakly stabilized by acetone, named Au solvated metal atoms (SMA). MVS approach offers the following advantages over conventional Au NPs synthesis: (i) size-controlled Au NPs are stabilized by the weakly interaction with the solvent (acetone) at room temperature (ii) Au NPs of comparable size are accessible, regardless of the support employed and the Au content; (iii) the supported Au NPs contain only metal in its reduced form avoiding further reduction or activation steps at high temperature; (iv) no by-products deriving from reduction steps are present [48-50].

The Au NPs were loaded onto the TNTAs surface by simply dipping the samples into the Au-acetone SMA solution. The Au NPs interacted with the superficial free titanols groups (i.e. hydroxyl groups) and were adsorbed on the solid TNTAs surface.

In order to evaluate the effect of the dipping time on the final Au loading, different experiments were carried out ranging between 2 and 1200 minutes (20 hours). The obtained samples were then acid digested and analysed by ICP-OES in order to evaluate their Au content. The Au loading was referred to the exposed geometric area (Fig. 1). As expected, high loadings came from long dipping times along a near exponential trend. At long dipping times (> 480 minutes, S5 and S6) a saturation of the TNTAs support was observed; noteworthy, more than half of this amount was raised after 120 minutes (S3) and almost one quarter of it after 10 minutes only (S2).

The non-linear metal loading trend obtained by increasing the dipping time is consisted with previously described interaction between MVS-derived metal NPs and the surface of metal oxide supports [46,51]. Briefly, at time zero all the titanols groups are free along with a large excess of available Au Nps in SMA solution, while during the deposition, free titanols sites decrease in view of still a large numbers of loaded NPs. Thus, a fast NPs deposition occurs at short reaction times and a decrease of deposition efficiency was expected at long dipping times.

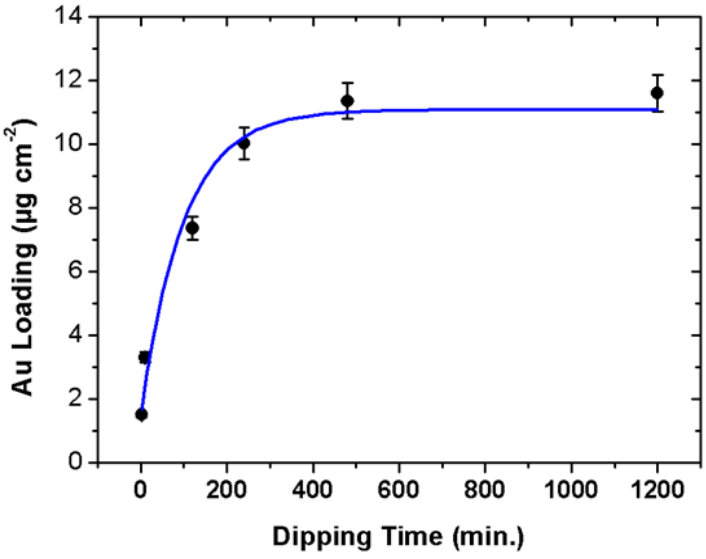

	Dipping time (min)	Au loading (µg cm^{-2})
S1	2	1.5 ± 0.05
S2	10	3.3 ± 0.2
S3	120	7.4 ± 0.4
S4	240	9.8 ± 0.5
S5	480	11.4 ± 0.6
S6	1200	11.6 ± 0.6

UNCORRECTED and UNAPPROVED version (submitted manuscript)

For the final, citable paper please see https://doi.org/10.1021/acsami.6b11436

Fig. 1. Au loading against dipping time of the TNTAs into Au-acetone SMA solution. Error bars for Au loading (as reported on the table on the right) correspond to ±5%.

The morphological features of Au/TNTAs composites were investigated by SEM, STEM and HRTEM analyses. SEM micrographs of the top-view of S2 and S6 samples (Fig. 2) revealed a highly homogeneous Au NPs dispersion without the presence of large Au aggregates. Particles coalescence were often reported using colloidal methodologies applied on flat surfaces [14, 52] leading to the formation of Au NPs islands with size larger than 50 nm. However, in our case these aggregation phenomena were not observed. The peculiar morphologies of TNTAs coupled with a strong interaction between the Au NPs and the TiO_2 surface, limited the NPs free mobility at room temperature ensuring a high metal dispersion. Indeed, the high surface area is distributed over not-connected nanotubes and the active titanol-coordinative sites are well separated avoiding long-range self-diffusion. Moreover, as expected, an increase of Au NPs amount was observed along with the long dipping time (Fig. S5).

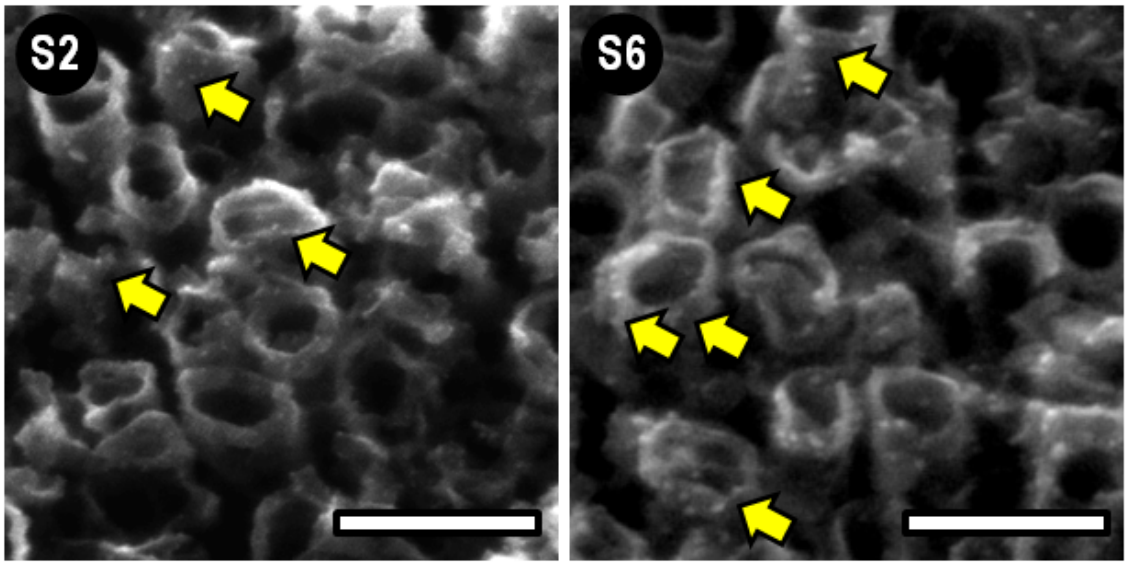

Fig. 2. Representative SEM micrographs of S2 (left side) and S6 (right side) samples. Scale bar: 200 nm. The arrows highlight examples of Au Nps location.

SEM-EDX data collected on selected samples (Table S1) showed a 3.4 ratio between Au contents for sample S6/S2(i.e samples obtained at 1200 and 10 minutes, respectively) such as the calculated ratio from ICP-OES analysis.

STEM and HRTEM analysis (Fig. 3) confirmed the presence of crystalline and well-shaped Au NPs. The STEM micrographs revealed Au NPs decorate both the outer and inner surface of the TiO_2 nanotubes (TNTs) on the tubes head or in the interstitial empty space between them.

UNCORRECTED and UNAPPROVED version (submitted manuscript)

For the final, citable paper please see https://doi.org/10.1021/acsami.6b11436

Moreover, Au NPs were randomly dislocated along all the tubes lengths (or rather along the tube fragments). HRTEM and STEM micrographs pointed out a slightly Au NPs warp as a consequence of a strong metal-support interaction. Looking at the particle dispersion for samples S1, S2, S4 and S6 (Fig. S6), the median values of size distributions were centred around 8 nm indicating no significant changes of Au NPs size distributions
till a dipping time of 480 minutes (sample S5). Only a small broadening in Au NPs size was observed for sample S6 which could be ascribed to a slightly NPs aggregation occurring at long dipping times (20 hours).

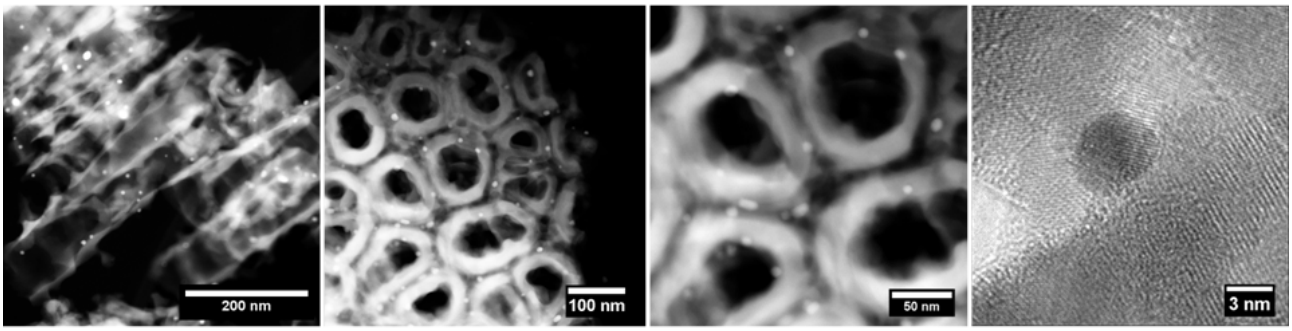

Fig. 3. Representative STEM micrographs and HRTEM (last micrograph) of sample S2.

In order to study the surface composition and chemical state of Au/TNTAs composites, XPS analysis of the different samples were performed. XPS survey spectra spectra of bare TNTAs, S2 and S6 samples (Fig. S7) showed peaks located at ca 458.2 and 464.1 eV corresponding to Ti $2p_{3/2}$ and Ti $2p_{1/2}$ of TiO_2. High-resolution spectrum of the Au $4f_{5/2}$ and Au $4f_{7/2}$ region of sample S6 revealed the core line centered at 82.9 eV($4f_{7/2}$) and the spin orbit separations (Δ) of 3.6 eV (Fig. S8), indicating the only presence of the metallic state Au^0 [53]. As previously reported by other authors, the negative shift recorded for Au^0 $4f_{7/2}$ with respect to reference pure Au foil (84 eV) demonstrate the strong metal-support interaction between the Au NPs and the TiO_2 support surface, according to that observed by electron microscopy analyses [54-55].
XRD analysis of bare TNTAs and representative S2 and S6 Au/TNTAs composites are reported in Fig. 4. All the samples showed diffraction peaks, which can be well indexed to anatase phase (JCPDS No. 86-1157) and metal titanium phase ascribed to the titanium foil support. In the XRD pattern of sample S6 containing the higher gold content a broad small peak located at 2θ 44,5° ca. (see the inset in Fig 5) that can be indexed for Au metal phase (JCPDS No. 04-0784), was observed.

UNCORRECTED and UNAPPROVED version (submitted manuscript)

For the final, citable paper please see https://doi.org/10.1021/acsami.6b11436

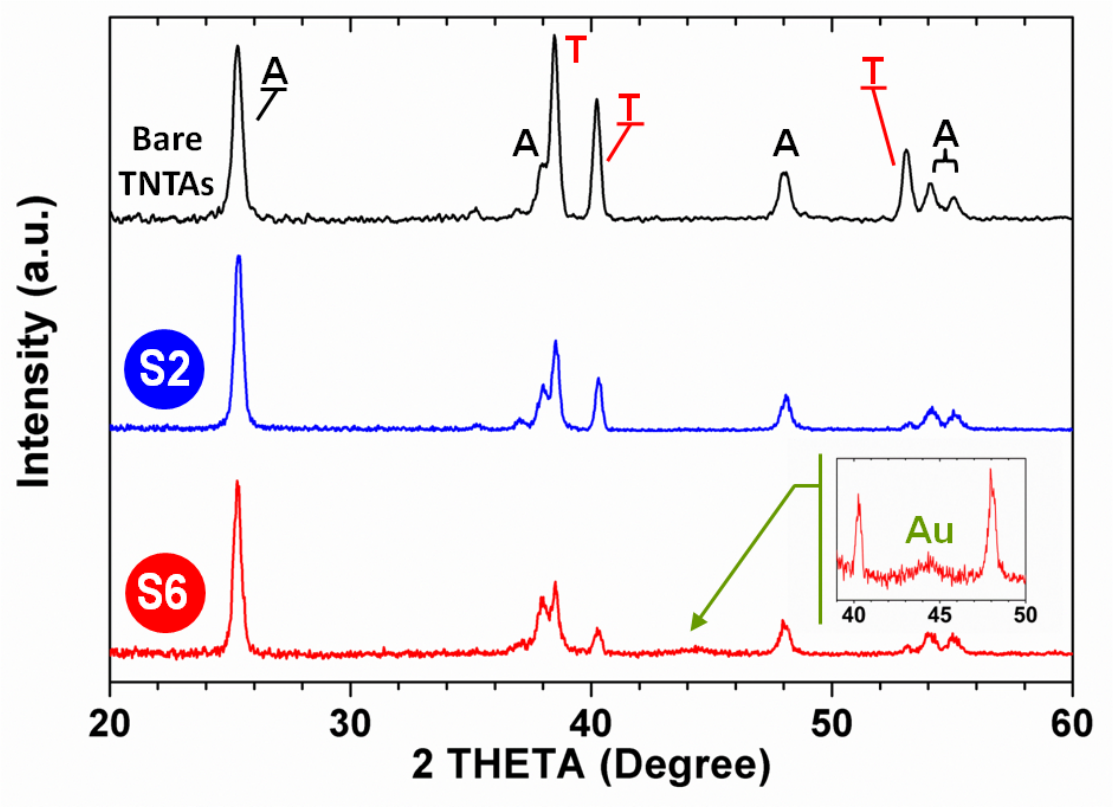

Fig. 4. -XRD patterns of bare TNTAs before Au deposition (black line, first row); sample S2 (blue line, in the middle row); sample S6 (red line, on the bottom row) and related pattern enlargement around Au peak at 2θ 44,5°. Patterns were indexed for TiO_2 anatase phase (A), metal titanium phase (T) and gold metal phase (Au).

UV−Vis diffuse reflectance spectra (Fig. S9) on samples showed a signal red shift after Au decoration, extending the absorption region towards the visible light. Moreover, for sample S6, thanks to the high metal loading, the gold plasmonic absorption peak at 550 nm was clearly detected whereas for other samples this peak is not so marked.

The photocatalytic activity of the Au/TNTAs samples, measured as toluene degradation reaction rate (as defined in ESI), is reported in Fig. 5a as absolute values for each sample before and after the Au NPs deposition. The relative variation of the photocatalytic activity of each specimen after Au NPs deposition is also reported versus the respective Au loading (Fig. 5b). The activity of the pristine batch of bare TNTAs slide was quite homogeneous and a marked increase of activity after Au NPs deposition was observed for the samples S2 and S3 containing Au loadings of 3.3 and 7.4 μg cm^{-2}, respectively. In particular, a three times increase of the activity for sample S2 and a two-time increase for S3 was detected. At lower Au loadings (S1 < 2 μg cm^{-2}) the reaction rate was

UNCORRECTED and UNAPPROVED version (submitted manuscript)

For the final, citable paper please see https://doi.org/10.1021/acsami.6b11436

comparable to the untreated sample whereas at higher loading (S6 > 10 μg cm^{-2}) a pronounced deactivation was observed.

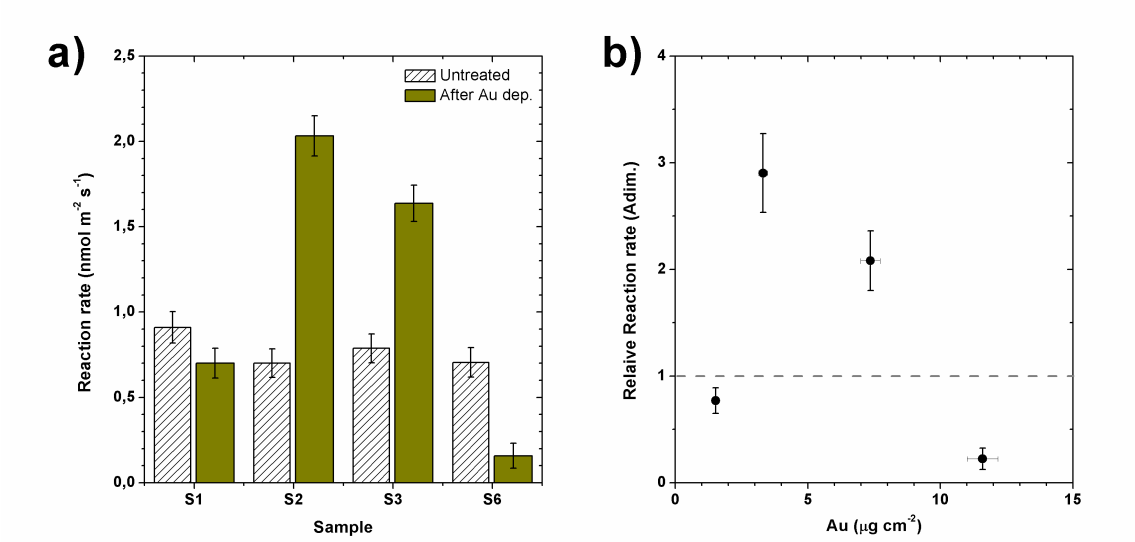

Fig. 5. -Toluene degradation rates: a) absolute reaction rate for each sample before and after Au NPs deposition; b) relative reaction rate for each sample after Au NPs deposition *vs.* Au loading. Dashed line indicates no effect (1:1 ratio). Error bars as 1 σ estimated repeatability error.

Although several research groups studied the effect of Au NPs on the photocatalytic activity of TiO_2-based materials, only few works deal with the use of TNTAs loaded with Au NPs in photo-degradation processes, particularly of airborne pollutants at typical ambient conditions. The effect of Au and Ag NPs on TNTAs was reported by Paramasivam *et al.* [37] confirming that the enhancing effect of metal NPs in water-based oxidative processes can also be exploited in case of highly organized titania nanostructures. Huang *et al.* [32] also studied TNTAs decorated with Au in the degradation of Rhodamine B. They found a maximum activity with a 0.68 wt.% Au loading, using visible-light irradiation. The degradation of benzene at high concentration in air (0.7-3.0 mol.%) with titania nanotubes modified by Au nanoparticles was studied by Awate *et al.* [56] confirming the activity enhancing effect of Au at low loadings (~ 1 wt.%) also in case of unsupported titania nanotubes.

The present study demonstrates the enhancement effect of Au NPs deposited on highly ordered supported nanotubes from a ligand-free Au-acetone SMA solution in the degradation of toluene at ambient concentration (i.e. in the ppb range). The photocatalytic enhancement effect of the deposited Au NPs agrees with the formation of a Schottky barrier at Au/TiO_2 interface that slows down the recombination of the photogenerated electron/hole pairs by separating the electron (that is preferentially transferred to the metallic nanoparticle) from the hole [14, 57]. The reduction of the

UNCORRECTED and UNAPPROVED version (submitted manuscript)

For the final, citable paper please see https://doi.org/10.1021/acsami.6b11436

competitive recombination reaction results in enhancement of the redox reactions with the chemical species available at the catalyst surface (Fig. S10). The alternative electron injection from the Au nanoparticle to the TiO_2 conduction band is sometime invoked [14, 22, 57, 58] when is operating the excitation of the Au surface plasmon band (~550 nm), but in the present study the use of UV-A radiation (365 nm) rules out this mechanism. The three-time factor activity enhancement with the optimal Au loading is comparable in magnitude to the results reported in literature with different Au-decorated catalytic systems (e.g. P25, titania layers or titania unsupported nanotubes) or with very different reaction conditions (e.g. degradation of pollutants in water or high concentrated pollutants in air) [19, 41, 59, 60]. The data available in literature do not allow a direct comparison of the absolute activity values in the different cases. It is nevertheless worth noting that the relative activity gain at the optimal Au loading found in the reported studies is comparable in magnitude despite the very different conditions used, supporting the existence of a common mechanism. Moreover, the enhancement factor obtained in this work with the deposition from ligand-free Au SMA solution is better than those reported in literature for gas-solid oxidative degradation processes and is equivalent to the best ones found for water-based systems.

In the present study it was found a maximum activity enhancement for the 3.3 μg cm^{-2} Au loaded sample and a net activity degradation (< 25% of the pristine sample) for the higher loaded sample (11.5 μg cm^{-2}). This is in clear agreement with previously reported studies [59, 60] indicating that the Au loading is a critical parameter for system efficiency. At relatively high loadings Au nanoparticles could mask the active titanol groups of titania surface giving an overall deactivation [57, 60]. Finally, the role of a post-deposition mild thermal treatment was investigated heating up sample S2 at 120°C for 30 minutes. A marked shift in the Au NPs size distribution, centred now around a median value of 13 nm (only the 17% of the NPs are < 10 nm in size), was observed leading to a decrease in the formal particles number (Fig. S11a). On the other hand, no morphological changes were detected for the TNTAs support. Interestingly, the activity dropped down slightly above the basal value (Fig. S11b) pointing out the role of Au NPs size and particle surface numerical density on the photocalytic behaviour of the AuNPs/TNTAs composites.

These results confirm that the loading and the size of Au NPs are critical for the optimization of the photocatalytic activity of TNTAs and that they must be finely tuned in order to maximize the photocatalytic system efficiency.

Conclusions

UNCORRECTED and UNAPPROVED version (submitted manuscript)

For the final, citable paper please see https://doi.org/10.1021/acsami.6b11436

Small Au NPs with controlled size were successfully loaded onto vertically aligned anatase TNTAs by a new synthetic protocol at room temperature avoiding further thermal treatments which could induce Au NPs aggregation as well as crystal and morphological TNTAs modifications. Au NPs were synthesized by means metal vapor synthesis technique affording ligand-free Au-acetone SMA solutions without the use of any surfactant or stabilizing agent. The metal NPs were easily deposited dipping the TNTAs support into the Au-acetone solution. The Au loadings were finely tuned ranging from 1.5 to 11.6 μg cm^{-2} by controlling the support/Au dipping time without significant change of Au NPs mean size. SEM, STEM, HRTEM and XPS analysis evidenced the presence of Au NPs with a mean size less than 10 nm highly dispersed on the TNTAs support and with a strong particles/support interaction. The photocatalytic activity of the Au/TNTAs composites was evaluated measuring the toluene degradation, as model substrate, in air at ambient conditions, demonstrating the efficacy of these systems also at very low pollutant concentration. The Au loadings strongly influenced the photocatalytic performances: the best performance resulting in a three times enhancement of the pristine TNTAs activity were obtained with a sample containing 3.3 μg cm^{-2} of Au. The proposed protocol could provide a new approach for the deposition of size-controlled metal NPs onto planar supports enabling the design of innovative composites for catalytic and photocatalytic applications.

UNCORRECTED and UNAPPROVED version (submitted manuscript)

For the final, citable paper please see https://doi.org/10.1021/acsami.6b11436

Reference

[1] Ji, P.; Takeuchi, M.; Cuong, T.-M.; Zhang, J.; Matsuoka, M.; Anpo, M. Recent Advances in Visible Light-Responsive Titanium Oxide-Based Photocatalysts. Res. *Chem. Intermediat.* **2010**, 36 (4), 327–347.

[2] Nakata, K.; Fujishima, A. TiO_2 Photocatalysis: Design and Applications. *J. Photochem. Photobiol. C Photochem. Rev.* **2012**, 13 (3), 169–189.

[3] Ma, Y.; Wang, X.; Jia, Y.; Chen, X.; Han, H.; Li, C. Titanium Dioxide-Based Nanomaterials for Photocatalytic Fuel Generations. *Chem. Rev.* **2014**, 114 (19), 9987–10043.

[4] Lin, J.; Liu, X.; Zhu, S.; Chen, X. TiO2 Nanotube Structures for the Enhancement of Photon Utilization in Sensitized Solar Cells. *Nanotechnol. Rev.* **2015**, 4 (3).

[5] Ola, O.; Maroto-Valer, M.M. Review of Material Design and Reactor Engineering on TiO_2 Photocatalysis for CO_2 Reduction. J. Photochem. Photobiol. C: Photochem. Rev. **2015**, 24, 16–42.

[6] Verbruggen, S. TiO_2 Photocatalysis for the Degradation of Pollutants in Gas Phase: From Morphological Design to Plasmonic Enhancement. *J. Photochem. Photobiol. C: Photochem. Rev.* **2015**, 24, 64–82.

[7] Karapati, S.; Giannakopoulou, T.; Todorova, N.; Boukos, N.; Antiohos, S.; Papageorgiou, D.; Chaniotakis, E.; Dimotikali, D.; Trapalis, C. TiO2 Functionalization for Efficient NOx Removal in Photoactive Cement. *Appl. Surf. Sci.* **2014**, 319, 29–36.

[8] Mo, J.; Zhang, Y.; Xu, Q.; Lamson, J.; Zhao, R. Photocatalytic Purification of Volatile Organic Compounds in Indoor Air: A Literature Review. *Atmosph. Environ.* **2009**, 43 (14), 2229–2246.

[9] Wang, S.; Ang, H.; Tade, M. Volatile Organic Compounds in Indoor Environment and Photocatalytic Oxidation: State of the Art. *Environ. Int.* **2007**, 33 (5), 694–705.

[10] Folli, A.; Pade, C.; Hansen, T.; Marco, T.; Macphee, D. TiO_2 Photocatalysis in Cementitious Systems: Insights into Self-Cleaning and Depollution Chemistry. *Cement Concrete Res.* **2012**, 42 (3), 539–548.

[11] Xu, A.-W.; Gao, Y.; Liu, H.-Q. The Preparation, Characterization, and Their Photocatalytic Activities of Rare-Earth-Doped TiO_2 Nanoparticles. *J. Catal.* **2002**, 207 (2), 151–157 .

[12] Liu, L.; Chen, X. Titanium Dioxide Nanomaterials: Self-Structural Modifications. *Chem. Rev.* **2014**, 114(19), 9890–918.

[13] Subramanian, V.; Wolf, E.; Kamat, P. Catalysis with TiO_2/Gold Nanocomposites. Effect of Metal Particle Size on the Fermi Level Equilibration. *J. Am. Chem. Soc.* **2004**, 126 (15), 4943–4950.

UNCORRECTED and UNAPPROVED version (submitted manuscript)

For the final, citable paper please see https://doi.org/10.1021/acsami.6b11436

[14] Primo, A.; Corma, A.; García, H. Titania Supported Gold Nanoparticles as Photocatalyst. *Phys. Chem. Chem. Phys.* **2011**, 13 (3), 886–910.

[15] Naldoni, A.; Fabbri, F.; Altomare, M.; Marelli, M.; Psaro, R.; Selli, E.; Salviati, G.; Santo, V. The Critical Role of Intragap States in the Energy Transfer from Gold Nanoparticles to TiO_2. *Phys. Chem. Chem. Phys.* **2015**, 17 (7), 4864–4869.

[16] Ding, D.; Liu, K.; He, S.; Gao, C.; Yin, Y. Ligand-Exchange Assisted Formation of Au/TiO2 Schottky Contact for Visible-Light Photocatalysis. *Nano Lett.* **2014**, 14 (11), 6731–6736.

[17] Naldoni, A.; D'Arienzo, M.; Altomare, M.; Marelli, M.; Scotti, R.; Morazzoni, F.; Selli, E.; Santo, V. Pt and Au/TiO_2 Photocatalysts for Methanol Reforming: Role of Metal Nanoparticles in Tuning Charge Trapping Properties and Photoefficiency. *Appl. Catal. B: Environ.* **2013**, 130, 239–248.

[18] Murdoch, M.; Waterhouse, G.; Nadeem, M.; Metson, J.; Keane, M.; Howe, R.; Llorca, J.; Idriss, H. The Effect of Gold Loading and Particle Size on Photocatalytic Hydrogen Production from Ethanol over Au/TiO_2 Nanoparticles. *Nat. Chem.* **2011**, 3(6), 489–92.

[19] Tanabe, I.; Ryoki, T.; Ozaki, Y. The Effects of Au Nanoparticle Size (5–60 nm) and Shape (sphere, Rod, Cube) over Electronic States and Photocatalytic Activities of TiO_2 Studied by Far- and Deep-Ultraviolet Spectroscopy. *RSC Adv.* **2015**, 5(18), 13648–13652.

[20] Bian, Z.; Tachikawa, T.; Zhang, P.; Fujitsuka, M.; Majima, T. Au/TiO_2 Superstructure-Based Plasmonic Photocatalysts Exhibiting Efficient Charge Separation and Unprecedented Activity. *J. Am. Chem. Soc.* **2013**, 136 (1), 458–65.

[21] Rayalu, S.; Jose, D.; Mangrulkar, P.; Joshi, M.; Hippargi, G.; Shrestha, K.; Klabunde, K. Photodeposition of AuNPs on Metal Oxides: Study of SPR Effect and Photocatalytic Activity. *Int. J. Hydrog. Energy* **2014**, 39(8), 3617–3624.

[22] Naldoni, A.; Riboni, F.; Marelli, M.; Bossola, F.; Ulisse, G.; Carlo, A.; Píš, I.; Nappini, S.; Malvestuto, M.; Dozzi, M.; Psaro, R.; Selli, E.; Santo, V. Influence of TiO_2 Electronic Structure and Strong Metal–support Interaction on Plasmonic Au Photocatalytic Oxidations. *Catal. Sci. Technol.* **2016**, 6, 3220-3229.

[23] Xiao, F.-X.; Zeng, Z.; Liu, B. Bridging the Gap: Electron Relay and Plasmonic Sensitization of Metal Nanocrystals for Metal Clusters. *J Am Chem Soc* **2015**, *137* (33), 10735–10744.

[24] Li, W.-C.; Comotti, M.; Schüth, F. Highly Reproducible Syntheses of Active Au/TiO_2 Catalysts for CO Oxidation by Deposition–precipitation or Impregnation. *J. Catal.* **2006**, 237(1), 190–196.

UNCORRECTED and UNAPPROVED version (submitted manuscript)

For the final, citable paper please see https://doi.org/10.1021/acsami.6b11436

[25] Oros-Ruiz, S.; Zanella, R.; López, R.; Hernández-Gordillo, A.; Gómez, R. Photocatalytic Hydrogen Production by Water/methanol Decomposition Using Au/TiO_2 Prepared by Deposition-Precipitation with Urea. *J. Hazard. Mater.* **2013**, 263 Pt 1, 2–10.

[26] Hidalgo; Maicu, M.; Navío, J.; Colón, G. Effect of Sulfate Pretreatment on Gold-Modified TiO_2 for Photocatalytic Applications. *J. Phys. Chem. C* **2009**, 113 (29), 12840–12847.

[27] Yogi, C.; Kojima, K.; Takai, T.; Wada, N. Photocatalytic Degradation of Methylene Blue by Au-Deposited TiO_2 Film under UV Irradiation. *J. Mater. Sci.* **2008**, 44(3), 821–827.

[28] Chiarello, G.; Zuliani, A.; Ceresoli, D.; Martinazzo, R.; Selli, E. Exploiting the Photonic Crystal Properties of TiO_2 Nanotube Arrays To Enhance Photocatalytic Hydrogen Production. *ACS Catal.* **2016**, 6(2), 1345–1353.

[29] Pang, Y.; Lim, S.; Ong, H.; Chong, W. A Critical Review on the Recent Progress of Synthesizing Techniques and Fabrication of TiO_2-Based Nanotubes Photocatalysts. *Appl. Catal. A: Gen.* **2014**, 481, 127–142.

[30] Diamanti, M.V.; Ormellese, M.; Pedeferri, M.P. Application-Wise Nanostructuring of Anodic Films on Titanium: A Review. *J. Exp. Nanosci.* **2015**, 10(17), 1285–1308.

[31] Mohamed, A.; Rohani, S. Modified TiO2 Nanotube Arrays (TNTAs): Progressive Strategies towards Visible Light Responsive Photoanode, a Review. *Energy Environ. Sci.* **2011**, 4(4), 1065-1086.

[32] Huang, Q.; Gao, T.; Niu, F.; Chen, D.; Chen, Z.; Qin, L.; Sun, X.; Huang, Y.; Shu, K. Preparation and Enhanced Visible-Light Driven Photocatalytic Properties of Au-Loaded TiO_2 Nanotube Arrays. *Superlattice Microst.* **2014**,75, 890–900.

[33] Wu, L; Li, F; Xu, Y; Zhang, JW; Zhang, D; Li, G. Plasmon-Induced Photoelectrocatalytic Activity of Au Nanoparticles Enhanced TiO_2 Nanotube Arrays Electrodes for Environmental Remediation. *Appl. Catal. B: Environ.* **2015**, 164, 217-224.

[34] Diamanti, M.V.; Ormellese, M.; Marin, E.; Lanzutti, A.; Mele, A.; Pedeferri, M.P. Anodic titanium oxide as immobilized photocatalyst in UV or visible light devices. *J. Hazard. Mater.* **2011**, 186, 2103–2109

[35] Xiao, F. Self-Assembly Preparation of Gold Nanoparticles-TiO 2 Nanotube Arrays Binary Hybrid Nanocomposites for Photocatalytic Applications. *J Mater Chem* **2012**, *22* (16), 7819–7830. hybrid nanocomposites

[36] Strini, A.; Sanson, A.; Mercadelli, E.; Bendoni, R.; Marelli, M.; Santo, V.; Schiavi, L. In-Situ Anatase Phase Stabilization of Titania Photocatalyst by Sintering in Presence of Zr^{4+} Organic Salts. *Appl. Surf. Sci.* **2015**, 347, 883–890.

UNCORRECTED and UNAPPROVED version (submitted manuscript)

For the final, citable paper please see https://doi.org/10.1021/acsami.6b11436

[37] Paramasivam, I.; Macak, J. M.; Schmuki, P. Photocatalytic Activity of TiO_2 Nanotube Layers Loaded with Ag and Au Nanoparticles. *Electrochem. Commun.* **2008**, 10(1), 71–75.

[38] Xiao, F.-X.; Zeng, Z.; Hsu, S.-H.; Hung, S.-F.; Chen, H.; Liu, B. Light-Induced In Situ Transformation of Metal Clusters to Metal Nanocrystals for Photocatalysis. *Acs Appl Mater Interfaces* **2015**, *7* (51), 28105–28109.

[39] Evangelisti, C.; Schiavi, E.; Aronica, L.A.; Psaro, R.; Balerna, A.; Martra, G.; "Solvated Metal Atoms in the Preparation of Supported Gold Catalysts", in L. Prati, A. Villa (Eds.), "Gold Catalysis: Preparation, Characterization and Applications, Pan Stanford Publishing Pte. Ltd., Singapore, **2016**, pp.73-92.

[40] Strini, A.; Schiavi, L. Low Irradiance Toluene Degradation Activity of a Cementitious Photocatalytic Material Measured at Constant Pollutant Concentration by a Successive Approximation Method. *Appl. Catal. B: Environ.* **2011**, 103(1-2), 226–231.

[41] Lee, S.; Scott, J.; Chiang, K.; Amal, R. Nanosized Metal Deposits on Titanium Dioxide for Augmenting Gas-Phase Toluene Photooxidation. *J. Nanopart. Res.* **2008**, 11(1), 209–219.

[42] ASTM B265-13ae1, Standard Specification for Titanium and Titanium Alloy Strip, Sheet, and Plate, ASTM International, West Conshohocken, PA, **2013**, www.astm.org.

[43] Macak, J.M.; Sirotna, K.; Schmuki, P. Self-organized porous titanium oxide prepared in Na_2SO_4/NaF electrolytes, *Electrochim. Acta* **2005**, 50, 3679–3684.

[44] Aronica, L.; Schiavi, E.; Evangelisti, C.; Caporusso, A.; Salvadori, P.; Vitulli, G.; Bertinetti, L.; Martra, G. Solvated Gold Atoms in the Preparation of Efficient Supported Catalysts: Correlation between Morphological Features and Catalytic Activity in the Hydrosilylation of 1-Hexyne. *J. Catal.* **2009**, 266(2), 250–257.

[45] Marelli, M.; Naldoni, A.; Minguzzi, A.; Allieta, M.; Virgili, T.; Scavia, G.; Recchia, S.; Psaro, R.; Santo, V. Hierarchical Hematite Nanoplatelets for Photoelectrochemical Water Splitting. *ACS applied materials & interfaces* **2014**, 6 (15), 11997–2004.

[46] Klabunde, K.; Chapter 5 - Chapter 6, Clusters, and Nanoscale Particles, ACADEMIC PRESS, INC.: San Diego (CA), **1994**, pp 98-193.

[47] Lin, S.; Franklin, M.; Klabunde, K. Nonaqueous Colloidal Gold. Clustering of Metal Atoms in Organic Media. 12. *Langmuir* **1986**, 2(2), 259–260.

[48] Jose, D.; Sorensen, C.; Rayalu, S.; Shrestha, K.; Klabunde, K. Au-TiO2 Nanocomposites and Efficient Photocatalytic Hydrogen Production under UV-Visible and Visible Light Illuminations: A Comparison of Different Crystalline Forms of TiO2. *International Journal of Photoenergy* **2013**, *2013*, 1–10.

UNCORRECTED and UNAPPROVED version (submitted manuscript)

For the final, citable paper please see https://doi.org/10.1021/acsami.6b11436

[49] Casaletto, M.; Longo, A.; Venezia, A.; Martorana, A.; Prestianni, A. Metal-Support and Preparation Influence on the Structural and Electronic Properties of Gold Catalysts. *Appl. Catal. A: Gen.* **2006**, 302(2), 309–316.

[50] Raffa, P.; Evangelisti, C.; Vitulli, G.; Salvadori, P. First Examples of Gold Nanoparticles Catalyzed Silane Alcoholysis and Silylative Pinacol Coupling of Carbonyl Compounds. *Tetrahedron Lett*. **2008**, 49(20), 3221–3224.

[51] Yu, L.; Zhang, X.; Du, Z.; Wang, D.; Wang, S.; Wu, S. Preparation of Nano-Sized γ-Al_2O_3 Supported Iron Catalyst for Fischer-Tropsch Synthesis by Solvated Metal Atom Impregnation Methods. *J. Nat. Gas Chem.* **2007**, 16(1), 46–52.

[52] Tian, F.; Klabunde, K.; Nonaqueous gold colloids. Investigations of deposition and film growth on organically modified substrates and trapping of molecular gold clusters with an alkyl amine. *New J. Chem.* **1998**, 22, 1275-1283

[53] Xiao, F.-X.; Hung, S.-F.; Miao, J.; Wang, H.-Y.; Yang, H.; Liu, B. Metal-Cluster-Decorated TiO 2 Nanotube Arrays: A Composite Heterostructure toward Versatile Photocatalytic and Photoelectrochemical Applications. *Small* **2015**, *11*(5), 554–567.

[54] Li, H.; Bian, Z.; Zhu, J.; Huo, Y.; Li, H.; Lu, Y. Mesoporous Au/TiO2 Nanocomposites with Enhanced Photocatalytic Activity. *J Am Chem Soc* **2007**, *129* (15), 4538–9.

[55] Zhu, S.; Liang, S.; Gu, Q.; Xie, L.; Wang, J.; Ding, Z.; Liu, P. Effect of Au Supported TiO2 with Dominant Exposed {001} Facets on the Visible-Light Photocatalytic Activity. *Appl Catal B Environ* **2012**, *119*, 146–155.

[56] Awate, S.V.; Sahu, R.K.; Kadgaonkar, M.D.; Kumar, R.; Gupta, N.M. Photocatalytic Mineralization of Benzene over Gold Containing Titania Nanotubes: Role of Adsorbed Water and Nanosize Gold Crystallites. *Catal. Today* **2009**, 141(1-2), 144–151.

[57] Ayati, A.; Ahmadpour, A.; Bamoharram, F.; Tanhaei, B.; Mänttäri, M.; Sillanpää, M.A Review on Catalytic Applications of Au/TiO_2 Nanoparticles in the Removal of Water Pollutant. *Chemosphere* **2014**, 107, 163–174.

[58] Naldoni, A.; Riboni, F.; Guler, U.; Boltasseva, A.; Shalaev, V.M.; Kildishev, A.V. Solar-Powered Plasmon-Enhanced Heterogeneousm Catalysis. *Nanophotonics* **2016**, DOI: 10.1515/nanoph-2016-0018.

[59] Arabatzis, I.; Stergiopoulos, T.; Andreeva, D.; Kitova, S.; Neophytides, S.; Falaras, P. Characterization and Photocatalytic Activity of Au/TiO_2 Thin Films for Azo-Dye Degradation. *J. Catal.* **2003**, 220 (1), 127–135.

[60] Orlov, A.; Jefferson, D.; Tikhov, M.; Lambert, R. Enhancement of MTBE Photocatalytic Degradation by Modification of TiO_2 with Gold Nanoparticles. *Catal. Comm.* **2007**, 8(5), 821–824.

UNCORRECTED and UNAPPROVED version (submitted manuscript)

For the final, citable paper please see https://doi.org/10.1021/acsami.6b11436

Table of Contents Graphic

TiO_2 Nanotubes Arrays Loaded with Ligand-free Au Nanoparticles: Enhancement in Photocatalytic Activity

Marcello Marelli, Claudio Evangelisti*, Maria Vittoria Diamanti, Vladimiro Dal Santo, Maria Pia Pedeferri, Claudia Bianchi, Luca Schiavi and Alberto Strini